

# Block approximations for probabilistic mixtures of elementary cellular automata

Emilio N.M. Cirillo<sup>\*1</sup>, Giacomo Lancia<sup>†1</sup>, and Cristian Spitoni<sup>‡2</sup>

<sup>1</sup>Dipartimento di Scienze di Base e Applicate per l'Ingegneria, Sapienza Università di Roma, via A. Scarpa 16, I-00161, Roma, Italy.

<sup>3</sup>Institute of Mathematics, University of Utrecht, Budapestlaan 6, 3584 CD Utrecht, The Netherlands.

**Abstract.** Probabilistic Cellular Automata are a generalization of Cellular Automata. Despite their simple definition, they exhibit fascinating and complex behaviours. The stationary behaviour of these models changes when model parameters are varied, making the study of their phase diagrams particularly interesting. The block approximation method, also known in this context as the local structure approach, is a powerful tool for studying the main features of these diagrams, improving upon Mean Field results. This work considers systems with multiple stationary states, aiming to understand how their interactions give rise to the structure of the phase diagram. Additionally, it shows how a simple algorithmic implementation of the block approximation allows for the effective study of the phase diagram even in the presence of several absorbing states.

Keywords: Probabilistic cellular automata; Synchronization; Stationary measures; Block approximation.

## 1. Introduction

Probabilistic Cellular Automata (PCA) generalize deterministic Cellular Automata (CA) as a discrete-time Markov chains with state space obtained as the product of a single lattice site finite state space. The variables associated with the lattice sites are updated independently and simultaneously according with a single site probability distribution which depends on the configuration of a neighbourhood of the site at the previous time. Despite the simplicity of their stochastic evolution rules, PCA exhibit a large variety of dynamical behaviours and, for this reason, they are considered powerful modelling tools, see, e.g., [1] for a general introduction to the topic and [2,3] for recent biological applications.

In this paper, we study the stationary behaviour of a

particular class of PCA which are a probabilistic mixtures of Elementary Cellular Automata (ECA) [4,5], namely, one dimensional CA in which the state of a cell is described by a two-state variable whose actual value, either zero or one, depends on the previous state of the two neighbouring cells and on that of the cell itself. In this context, binary probabilistic mixtures, called *diploid*, have been widely studied in the recent literature [6], not only for their intrinsic interest, but also because some of them encode the evolution rule of very well known paradigmatic PCA models, such as the *percolation* [7,8], the *noisy additive* [9], the *Stavskaya* [10], and the *directed animals* PCA [11].

We will use block approximation techniques as the main tool of our analysis. The idea of approximating the stationary measure of the PCA via measures defined on blocks

<sup>\*</sup>emilio.cirillo@uniroma1.it

<sup>†</sup>giacomo.lancia@uniroma1.it

<sup>‡</sup>C.Spitoni@uu.nl

with a maximal controlled size dates back to the pioneering papers [12,13] in which the local structure of PCA was firstly investigated. More recently, this idea has been used to investigate the structure of the stationary measures of PCA in several contexts, for instance, in the case of asynchronous PCA [14].

In these applications, the block approximation is often implemented by writing analytic expressions for some quantity of interest [15,16]. In this work, we adopt an algorithmic scheme inspired by the Cluster Variation Method [17,18], which is commonly used for Statistical Mechanics systems. We emphasize that we do not look for optimization on the number of variables or for the analytic control of the computation, but we choose the maximal block and write recursive equations for the probabilities associated with each possible configuration on that block. The advantage is that we set a fully algorithmic procedure which, in principle, can be applied to any PCA. On the negative hand we, obviously, miss any analytical control on the computation which, additionally, becomes more and more time-consuming when the size of the maximal block is increased.

The aim of this paper is to show the ability of this basic implementation of the block approximation to describe the structure of the stationary measures of PCA in several contexts, in particular, in cases in which competition between contrasting behaviours makes the model complicated and not accessible by simple Mean Field techniques. More precisely, the goal is to use the block approximation to construct the phase diagram of the model, that is to say, to characterize the stationary measure of the model in the different regions of the parameter space and, in particular, to detect those points (or lines) where a transition between different stationary states is observed.

As the first goal, we consider the diploid, in which one of the two local rules is the null rule, namely the rule associating the zero state with any local configuration. These models will be called Null Diploid Elementary Cellular Automata (NDECA). Due to its interesting behaviour, this particular class of diploid has been extensively studied in [6] via Monte Carlo simulations and in [19] via Mean Field and rigorous one-site ergodicity criteria [20,21]. The Mean Field analysis is in general in very good agreement with the Monte Carlo results, but for some specific choices of

the non-null rule, the two methods are in disagreement on the existence of a transition or on its character. Here, we show that these discrepancies are resolved when approximations on blocks larger than three are considered. Moreover, looking at the block probability distribution, it is possible to understand why the Mean Field approximation fails in describing the diploid behaviour.

We remark that one of the characterizing traits of NDECA is that there exists at most one unique absorbing state, namely, the zero state, since cells with state one have a non-zero probability to be changed to zero. For this reason, in the second part of the paper we focus our attention on models in which, on the contrary, there exist at least two absorbing states. We will, thus, analyze how their contrasting effects affect the stationary behavior of the PCA and we will test the ability of our implementation of the block approximation to detect the structure of the phase diagram even in this intrinsically pernicious set-up.

We have chosen two models such that one of them can be written as a diploid, namely, a probabilistic mixture of two ECA, while the second one is a probabilistic mixture of four ECA. This second model is equivalent to an example of totalistic PCA, namely, a PCA in which the site updating probability depends only on the total of the values of the cells in a neighbourhood. In both cases, we show that the block approximation is able to provide a complete interpretation of the Monte Carlo results and to give a full description of the main features of the model. The two selected models are not new in the literature, and their interest have already been pointed out in [16,22].

The paper is organized as follows. We give the definition of a probabilistic mixture of ECA and introduce the block approximation in Section 2. We discuss the NDECA in Section 3, while the diploid and the four ECA mixture with two absorbing states are respectively discussed in Sections 4 and 5. Finally, in Section 6 we summarize our conclusions.

## 2. Model and methods

In this section, we first introduce the class of models which will be the object of our study and then we will discuss our main techniques.

### 2.1. Probabilistic mixtures of ECA

Given the *set of states*  $Q = \{0, 1\}$  and the  $n$  cell annulus  $\Lambda_n = \mathbb{Z}/n\mathbb{Z} = \{0, 1, \dots, n-1\}$ , with  $n$  an odd integer number, we consider the *configuration space*  $X_n = Q^{\Lambda_n}$ . For  $x \in X_n$ ,  $x_i$  is called the *value* of the cell  $i$  or the *occupation number* of the cell  $i$ . The configurations with all the cell states equal to zero (resp. one) will be simply denoted by 0 (resp. 1). For any  $x \in X_n$  and  $\Delta \subset \Lambda_n$ , we let  $x_\Delta$  be the restriction of  $x$  to  $\Delta$ .

In CA the cell states are updated synchronously according to the state the cells of the system. More precisely, given the map  $F : X_n \rightarrow X_n$ , the CA associated with  $F$  is the collection of all the sequences of configurations  $(\zeta^t)_{t \in \mathbb{N}}$  obtained by applying the map  $F$  iteratively, namely, such that  $\zeta^t = F(\zeta^{t-1})$ . The sequence  $(\zeta^t)_{t \in \mathbb{N}}$  such that  $\zeta^0 = x \in X_n$  is called *trajectory* of the CA with *initial condition*  $x$ .

A particular example of CA are the so-called ECA, in which the cell states are updated according to the state of the two neighbouring cells and that of the cell itself. These three cells form the neighbourhood of the cell, namely, the *neighbourhood of the cell*  $i \in \Lambda_n$  is the set  $I_i = \{i-1, i, i+1\}$ . Note that, due to the periodic structure of the lattice  $\Lambda_n$ , the neighbourhood of the origin is the set  $I_0 = \{n-1, 0, 1\}$ . Thus, given a *local rule*  $f : Q^3 \rightarrow Q$ , the associated ECA is the CA defined by the map  $F : X_n \rightarrow X_n$  such that  $(F(x))_i = f(x_{I_i})$ , for any  $i \in \Lambda_n$ .

We recall the classical notation for all the possible 256 ECA, see, e.g., [6, 19] and references therein: a local rule  $f$  is identified by the integer number  $W \in \{0, \dots, 255\}$  such that

$$\begin{aligned} W &= f(1, 1, 1) \cdot 2^7 + f(1, 1, 0) \cdot 2^6 + f(1, 0, 1) \cdot 2^5 \\ &\quad + f(1, 0, 0) \cdot 2^4 + f(0, 1, 1) \cdot 2^3 + f(0, 1, 0) \cdot 2^2 \\ &\quad + f(0, 0, 1) \cdot 2^1 + f(0, 0, 0) \cdot 2^0 \\ &= \sum_{i=0}^7 c_i \cdot 2^i. \end{aligned} \quad (2.1)$$

The last equality defines the coefficients  $c_i$  providing the binary representation of the number  $W$ . We shall sometimes denote the ECA with both the decimal and the binary representation by writing  $W(c_7c_6c_5c_4c_3c_2c_1c_0)$ . Note that for the given the ECA  $W$  as in (2.1), the *conjugate under left-right reflection* rule is obtained by exchanging  $f(1, 1, 0)$  with  $f(0, 1, 1)$  and  $f(1, 0, 0)$  with  $f(0, 0, 1)$ .

The stochastic generalization of CA are called PCA and are defined as a Markov Chain  $(\zeta^t)_{t \in \mathbb{N}}$  on the configuration space  $X_n$  with transition matrix

$$p(x, y) = \prod_{i \in \Lambda_n} p_i(y_i|x), \quad (2.2)$$

where  $p_i(\cdot|x)$ , called *one-site updating probability*, is a probability distribution on  $Q$  parameterized by the configuration  $x \in X_n$ . Thus, at each time all the cells are updated simultaneously and independently. We denote by  $P_x$  the probability associated with the process started at  $x \in X_n$ , so that,  $P_x(\zeta^t = y)$  is the probability that the chain started at  $x$  is in the configuration  $y$  at time  $t$  and  $= P_x(\zeta^t \in Y)$  is the probability that a chain started at  $x$  is in the set of configurations  $Y \subset X_n$  at time  $t$ .

In this paper, we will consider PCA defined as probabilistic mixtures of ECA, namely, we shall assume

$$p_i(y_i|x) = y_i\phi(x_{I_i}) + (1 - y_i)[1 - \phi(x_{I_i})], \quad (2.3)$$

where, given the positive integer  $m$ , the function  $\phi : Q^3 \rightarrow [0, 1]$  is defined as

$$\phi = \sum_{r=1}^m \xi_r f_r, \quad (2.4)$$

with  $\xi_r \in [0, 1]$  such that  $\sum_{r=1}^m \xi_r = 1$  and  $f_1, \dots, f_m$  are  $m$  local rules. It is important to note that the time evolution of a probabilistic mixtures of ECA can be described as follows: at time  $t$  for each cell  $i \in \Lambda_n$  one chooses one of the rules  $f_1, \dots, f_m$  with probability  $\xi_r$  and performs the updating based on the neighbourhood configuration at time  $t-1$ . Indeed, with this algorithm the probability to set the cell to 1 a time  $t$  is the sum of the  $\xi_r$  such that  $f_i$ , computed in the neighbourhood configuration at time  $t-1$ , is one.

In the case  $m = 2$ , which has been widely studied in the literature, see, e.g., [6, 19] and references therein, the probabilistic mixtures of ECA are called *diploid* and equation (2.4) is rewritten as

$$\phi = (1 - \lambda)f_1 + \lambda f_2, \quad (2.5)$$

with  $\lambda \in [0, 1]$ .

Finally, we remark that the function  $\phi : Q^3 \rightarrow [0, 1]$  can be interpreted as the probability to set the cell  $i$  to 1 given the neighbourhood configuration  $x_{I_i}$  and, similarly,  $1 - \phi$  is the probability of selecting 0.

## 2.2. Order parameter

We are interested in studying the possibility of PCA to exhibit multiple stationary behaviours. Given a measure  $\mu$  on  $Q$  which is stationary for the PCA, exploiting the translational invariance, we will characterize it by the average occupation number of the cell at the origin

$$\delta_\mu = \sum_{\substack{x \in X_n: \\ x_0=1}} \mu(x),$$

which will be called *density*.

Sometimes, we will explore the stationary behavior using Monte Carlo simulations. In such a case we will start the PCA from an initial configuration in which cells are randomly and uniformly populated with zeros and ones. Then, the density will be estimated by the large time behavior of the empirical average

$$\delta_x(t) = \frac{1}{n} \sum_{i \in \Lambda_n} \zeta_i^t. \quad (2.6)$$

## 2.3. Block approximation

We propose a block approximation scheme of the stationary measure of any PCA. With the term *block* we mean a sequence of contiguous cells.

Let us consider a block made of an odd number of contiguous cells, namely, the  $(2m+1)$ -block  $B_{i,m}$  is the set of cells  $\{i-m, i-m+1, \dots, i, \dots, i+m-1, i+m\}$ , with  $i \in \Lambda_n$  and  $1 \leq m \leq (n-1)/2$ ; recall  $\Lambda_n$  is an annulus and  $n$  is an odd integer number. Note that the neighborhood  $I_i$  defined above is nothing but the block  $B_{i,3}$ . Thus, given  $z$  a configuration on  $B_{i,m}$  we write

$$\begin{aligned} P_x(\zeta_{B_{i,m}}^t = z) &= \sum_{y \in X_n} P_x(\zeta_{B_{i,m}}^t = z | \zeta^{t-1} = y) P_x(\zeta^{t-1} = y) \\ &= \sum_{y \in X_n} \prod_{k=i-m}^{i+m} p_k(z_k | y) P_x(\zeta^{t-1} = y) \\ &= \sum_{y \in Q^{B_{i,m+1}}} \prod_{k=i-m}^{i+m} p_k(z_k | y) P_x(\zeta_{B_{i,m+1}}^{t-1} = y). \end{aligned} \quad (2.7)$$

Now, let  $\varrho$  be the stationary distribution. We slightly abuse the notation by defining:

$$\varrho(z) = \sum_{y \in \Lambda_n: y_{B_{i,m+1}} = z} \varrho(y) \quad (2.8)$$

for any  $z \in Q^{B_{i,m}}$ . Thus, by setting  $B_m = B_{0,m}$  and exploiting the translation invariance, from (2.7) we get

$$\varrho(z) = \sum_{y \in Q^{B_{m+1}}} \prod_{k \in B_m} p_k(z_k | y) \varrho(y) \quad (2.9)$$

for any  $z \in Q^{B_m}$ . We remark that the left-hand side of the equation above contains the  $2^{2m+1}$  values of the stationary probability of the configurations on the  $(2m+1)$ -block  $B_m$ . Instead, the right-hand side is written in terms of the  $2^{2m+3}$  values of the stationary probability of the configurations on the  $(2m+3)$ -block  $B_{m+1}$ .

When considering a block approximation, the probabilities associated with the block  $B_{m+1}$  are approximated by combinations of probabilities associated with smaller blocks. If we denote by  $P_\varrho$  these approximated block probabilities, the equations above can be closed to provide the approximated stationary maximal block probabilities as follows

$$\varrho(z) = \sum_{y \in Q^{B_{m+1}}} \prod_{k \in B_m} p_k(z_k | y) P_\varrho(y), \quad (2.10)$$

where we recall that  $z \in Q^{B_m}$ .

In the following we shall adopt the Bayes' rule for block approximation [12–14], namely,

$$P_\varrho(x_i x_{i+1}) = \varrho(x_i) \varrho(x_{i+1}), \quad (2.11)$$

and

$$P_\varrho(x_i \dots x_{i+k}) = \frac{\varrho(x_i \dots x_{i+k-1}) \varrho(x_{i+1} \dots x_{i+k})}{\varrho(x_{i+1} \dots x_{i+k-1})}, \quad (2.12)$$

for any  $i$  and  $k \geq 2$ . When the denominator vanishes, we assume  $P_\varrho(x_i \dots x_{i+k}) = 0$ .

In the applications that will be discussed in the following sections we shall use the approximation based on the maximal block of size  $k$ , for  $k = 3, 5, \dots, 13$ , which will be called  $k$ -block approximation. It is useful to write explicitly the recursive equation that we find at least for the smaller values of  $k$ . For the 3-block approximation we have

$$\begin{aligned} \varrho(z_{n-1} z_0 z_1) &= \sum_{y \in Q^{B_2}} p_{n-1}(z_{n-1} | y) p_0(z_0 | y) p_1(z_1 | y) \\ &\quad \times \varrho(y_{n-2} y_{n-1} y_0) \varrho(y_{n-1} y_0 y_1) \varrho(y_0 y_1 y_2) \\ &\quad \times \frac{\mathbb{1}_{\varrho(y_{n-1} y_0) \varrho(y_0 y_1) > 0}}{\varrho(y_{n-1} y_0) \varrho(y_0 y_1)}. \end{aligned} \quad (2.13)$$

For the 5-block approximation we have

$$\begin{aligned}
& \varrho(z_{n-2} \dots z_2) \\
&= \sum_{y \in Q^{B_3}} p_0(z_0|y) \prod_{k=1}^2 p_{n-k}(z_{n-k}|y) p_k(z_k|y) \\
&\quad \times \varrho(y_{n-3} \dots y_1) \varrho(y_{n-2} \dots y_2) \varrho(y_{n-1} \dots y_3) \\
&\quad \times \frac{\mathbb{1}_{\varrho(y_{n-2} \dots y_1) \varrho(y_{n-1} \dots y_2) > 0}}{\varrho(y_{n-2} \dots y_1) \varrho(y_{n-1} \dots y_2)}. \tag{2.14}
\end{aligned}$$

For the 7-block approximation we have

$$\begin{aligned}
& \varrho(z_{n-3} \dots z_3) \\
&= \sum_{y \in Q^{B_4}} p_0(z_0|y) \prod_{k=1}^3 p_{n-k}(z_{n-k}|y) p_k(z_k|y) \\
&\quad \times \varrho(y_{n-4} \dots y_2) \varrho(y_{n-3} \dots y_3) \varrho(y_{n-2} \dots y_4) \\
&\quad \times \frac{\mathbb{1}_{\varrho(y_{n-3} \dots y_2) \varrho(y_{n-2} \dots y_3) > 0}}{\varrho(y_{n-3} \dots y_2) \varrho(y_{n-2} \dots y_3)}. \tag{2.15}
\end{aligned}$$

For the 9-block approximation we have

$$\begin{aligned}
& \varrho(z_{n-4} \dots z_4) \\
&= \sum_{y \in Q^{B_5}} p_0(z_0|y) \prod_{k=1}^4 p_{n-k}(z_{n-k}|y) p_k(z_k|y) \\
&\quad \times \varrho(y_{n-5} \dots y_3) \varrho(y_{n-4} \dots y_2) \varrho(y_{n-3} \dots y_3) \\
&\quad \times \varrho(y_{n-2} \dots y_4) \varrho(y_{n-3} \dots y_5) \\
&\quad \times \frac{\mathbb{1}_{\varrho(y_{n-4} \dots y_3) \varrho(y_{n-3} \dots y_4) > 0}}{\varrho(y_{n-4} \dots y_3) \varrho(y_{n-3} \dots y_4)}. \tag{2.16}
\end{aligned}$$

Equations (2.13)–(2.16) will be solved using the scheme proposed in [23] within the framework of the Cluster Variation Method and called the Natural Iteration Method, see, also, [17]. More specifically, the initial  $m$ -block probabilities are chosen, and then, at each step of the iteration, the  $(m-1)$ -block probabilities are computed via symmetrized marginalization. Next, the equations (2.13)–(2.16) are then employed to compute the new  $m$ -block probabilities. This algorithm is repeated till a fixed point is reached. In general we fix an *a priori* precision of  $10^{-7}$  for the  $L^2$  norm of the  $m$ -block probabilities, but in some cases we shall discuss the dependence of the results on this parameter.

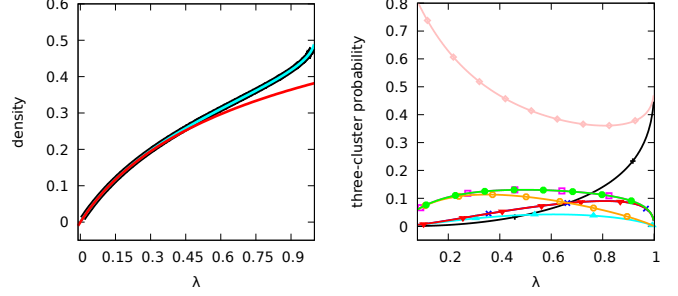


Figure 1: NDECA 17. On the left, stationary density versus  $\lambda$  computed via mean field theory (red), 3-block approximation (cyan), and Monte Carlo simulation (black). On the right, 3-block probability computed via the 3-block approximation:  $\varrho(111)$  (black, cross),  $\varrho(110)$  (blue, times symbol),  $\varrho(101)$  (cyan, up triangle),  $\varrho(100)$  (magenta, open square),  $\varrho(011)$  (red, down triangle),  $\varrho(010)$  (orange, open disk),  $\varrho(001)$  (green, solid disk),  $\varrho(000)$  (pink, diamond).

### 3. Null rule diploid elementary cellular automata

In this section we focus our attention on mixtures of two elementary cellular automata in which one of the two mixed local rules is the null rule. More in the definition (2.5) of the function  $\phi$  the map  $f_1$  is the null rule (i.e., the local rule  $W = 0$ ) and  $f_2$  is any other local rule. As mentioned in the Introduction, following [19], we refer to these kinds of diploid as NDECA and denote by NDECA  $W$  the NDECA whose  $f_2$  map is the local rule  $W$ .

We remark that the measure concentrated on the configuration 0 is the unique invariant measure for the finite-volume NDECA in the cases in which the  $f_2$  rule is even. Indeed, whatever is the configuration, cells with state one have a non-zero probability (at least  $1 - \lambda$ ) to be changed to zero. Thus, if the zero rule is predominant, we expect a stationary measure essentially concentrated on the zero state. On the other hand, depending on the second local rule used in the mixtures, for  $\lambda$  large enough, different behaviors can emerge. Thus, as discussed in [6, 19], the main question is to understand if in the infinite-volume limit, namely,  $n \rightarrow \infty$ , a different stationary measure exists, with a positive value of the average cell occupation number.

As mentioned in the Introduction, this problem has been extensively studied in [6] via numerical simulations

and in [19] via Mean Field approximation and rigorous one-site criteria. We shall approach here the problem by means of the block approximation for some particular NDECA of interest. More specifically, we shall discuss those cases in which the Mean Field and the numerical predictions are not in agreement. All Monte Carlo results discussed in this section are obtained on the annulus  $\Lambda_n$  with  $n = 10^5$  considering  $2 \times 10^5$  full updates of the lattice starting from a random initial configuration chosen with a Bernoulli distribution of parameter  $1/2$ .

In [19] a detailed study of the Mean Field approximation has been provided and, in particular, it was proven that, within such an approximation, odd NDECA have a unique stationary state. Such a result is consistent with the Monte Carlo study of [6].

The investigation of the particular case of the NDECA 17 via 3 and 5-block approximations confirmed the absence of a phase transition. Incidentally, such a NDECA is known as the *directed animals* PCA (see for instance Figure 7 in [9]) and it has been proven to have a unique invariant *Markovian* measure. The left panel of Figure 1 shows density as a function of  $\lambda$ . Results from the Mean Field match perfectly with those obtained using the 3-block approximation. In the picture we have not reported graphs obtained with higher order block approximations, since they match perfectly with the 3-block approximation prediction.

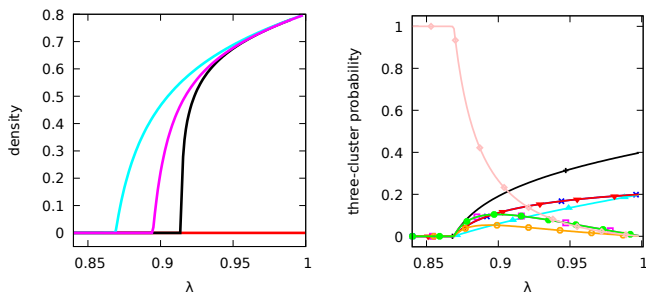


Figure 2: As in Figure 1 for NDECA 202. In the left panel the magenta line refers to the 5-block approximation

When considering even NDECA, Mean Field results are more interesting, even if less precise. As reported in [19] within this approximation the non-uniqueness of the stationary measure is correctly predicted for all the models for which the simulation study of [6] revealed this behavior, except for the NDECA 202.

As reported in Figure 2, the existence of stationary measure not concentrated on 0 is captured by the block approximations and the estimate of the value of the critical  $\lambda$  gets closer to the Monte Carlo result as the order of the approximation is increased.

In the right panel of Figure 2, we report the 3-block probability computed via the 3-block approximation. It is interesting to remark that at large values of  $\lambda$  the 3-block probability does not concentrate on the 111 configuration. This explains why Mean Field is not able to capture the transition.

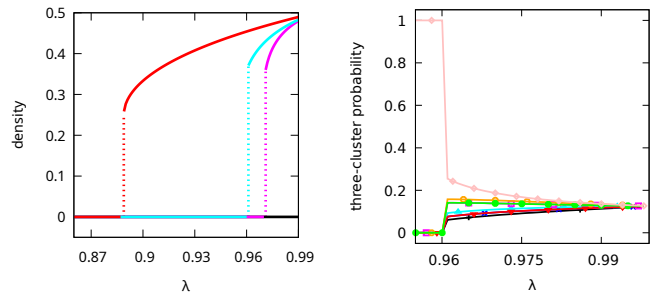


Figure 3: As in Figure 2 for NDECA 120.

On the other hand, there are also cases where the Mean Field theory predicts the existence of a transition that is not observed in Monte Carlo simulations, such as in the case of NDECA 120. As reported in Figure 3, the Mean Field predicts a discontinuous transition, which is confirmed by the block approximations, but only for values of  $\lambda$  very close to unity. This evidence, together with the fact that all 3-block probabilities converge to the same value for  $\lambda$  large (see the graphs on the right panel of the same figure), strongly suggests that this is an artifact of the block approximations.

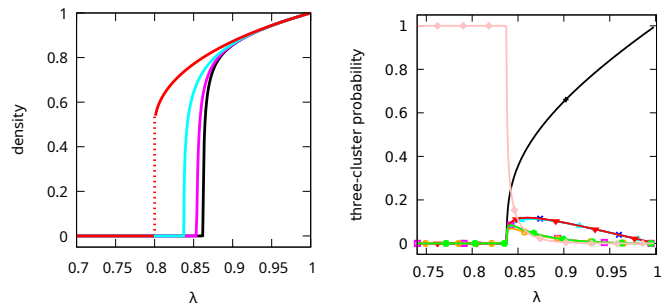


Figure 4: As in Figure 2 for NDECA 234.

Mean Field approximation finds a discontinuous transition also for NDECA 234, for which Monte Carlo simulation predicts the existence of a continuous transition. As illustrated in Figure 4, the block approximations recover a continuous transition and, as already remarked in a similar case, the estimate of the critical value of  $\lambda$  gets closer and closer to the Monte Carlo prediction when the order of the block approximation is increased. It is also worth noting that the Mean Field and the block approximation estimate of the density matches the Monte Carlo prediction perfectly for large  $\lambda$ : this is the case when the block probabilities concentrate on the configuration 111, as shown in the right panel of the figure.

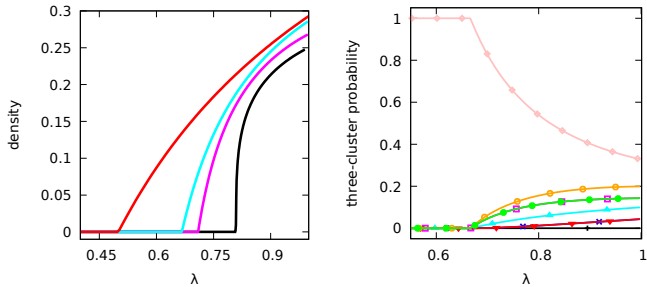


Figure 6: As in Figure 2 for NDECA 18.

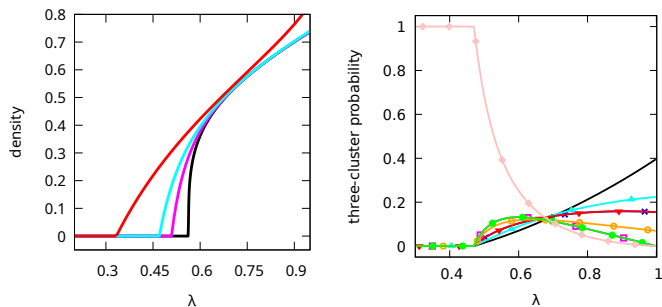


Figure 5: As in Figure 2 for NDECA 222.

As reported in [19], Mean Field also predicts the existence of the transition for the NDECA 222, a phenomenon not investigated in [6]. This is confirmed by the results of Figure 5. Interestingly, we remark that the density profile at large  $\lambda$  is not well reproduced through the Mean Field, whereas a perfect match is recovered when block approximations are considered. As noticed, this is imputed to the fact that when  $\lambda$  is close to one the 3-block probabilities do not concentrate on 111; see the right panel of Figure 5. Such a situation is not easily captured by Mean Field. Indeed, the main limit of the Mean Field approximation is due to the fact that the equation providing the stationary density depends only on the total number of configurations with a fixed number of ones that associate 1 to the configuration in the neighborhood under the map  $f$ .

We now pass to discuss other useful examples to illustrate how the block approximation works. The ECA 18 is a chaotic CA belonging to Wolfram’s class  $W3$ ; it is also called *diffusive rule*. The main feature of ECA 18 is that at time  $t$  it updates a central site with a one only if at time  $t - 1$  there is a one either on its left or on its right. Thus, it is an example of a symmetric rule. Figure 6 shows that also this NDECA does not concentrate, for  $\lambda$  close to unity, the 3-block probabilities on the outcome 111. As a consequence, the Mean Field prediction is not particularly satisfactory, whereas larger block approximations are able to predict a density profile that gets closer and closer to the Monte Carlo result. It is worth noting that this diploid is particularly challenging for the block approximations, as shown by the graphs in the left panel of the figure, since the 111 block configuration does not contribute to the stationary density while all the other 3-block configurations have not zero stationary probability.

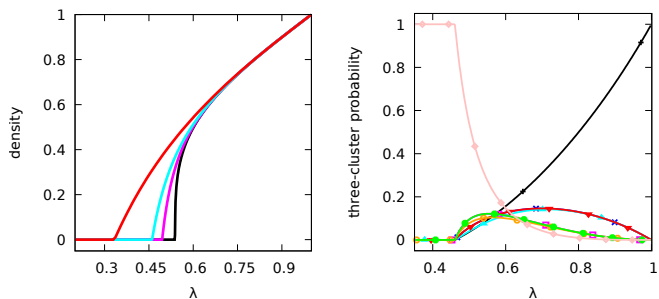


Figure 7: As in Figure 2 for NDECA 254.

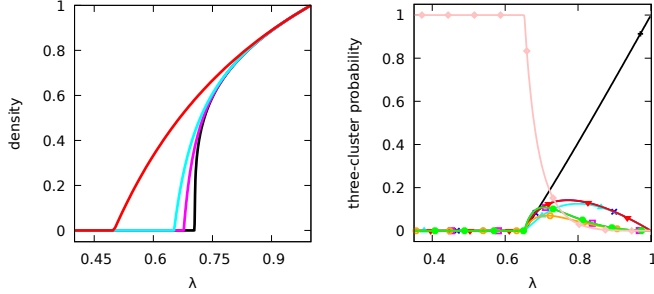


Figure 8: As in Figure 2 for NDECA 238.

The NDECA 254 is based on the simple rule 254, which has the configuration with all ones as fixed point (Wolfram’s class  $W1$ ). For this diploid, see Figure 7. The Mean Field prediction and the Monte Carlo results compare very well far from the critical point. Once again, this is due to the fact that for a  $\lambda$  close to unity the block probabilities concentrate on 111. This diploid is well known in the literature, see, e.g., [7, 8], where it is called *percolation PCA*. In [7, Example 2.4] the existence of the transition is proven rigorously. The exact value of the critical  $\lambda$  is not known, but it is proven that it belongs to the interval  $[1/3, 53/54]$ , see [8]. In [24] the lower bound 0.505 is given. Mean Field, 3–block, and 5–block approximations, respectively, predict  $1/3$ ,  $0.461 \pm 0.001$ , and  $0.496 \pm 0.001$ . For the block approximations, we take as the operative definition of critical  $\lambda$  the value such that the density is larger than 0.01.

As a last example, we consider the NDECA 238, whose behavior, very similar to that of NDECA 254, is reported in Figure 8. This NDECA is called the *Stavskaya* model and it is a particular case of the *percolation PCA*. For the critical value of  $\lambda$ , the lower bound is 0.677 (see [20]). Mean Field, 3–block, and 5–block approximations respectively predict 0.5,  $0.654 \pm 0.001$ , and  $0.678 \pm 0.001$ .

#### 4. A diploid with two absorbing states

In this section, we consider the diploid obtained as a mixtures of the local rules  $W = 200$  and  $W = 182$  [16], see Table 4.1. More precisely, the model is defined by the equations (2.2), (2.3), and (2.5) where  $f_1$  is the local rule 200 and  $f_2$  the local rule 182. The dynamics becomes deterministic as  $\lambda$  assumes the values 0 and 1 and, in particular, it reduces to the ECA 200 and 182, respectively.

As mentioned above, we use our algorithmic implementation of the block approximation to study the phase diagram of the model and we show that, provided the size of the maximal block is sufficiently large, the main features of the Monte Carlo results are fully recovered.

	111	110	101	100	011	010	001	000
<b>200</b>	1	1	0	0	1	0	0	0
<b>182</b>	1	0	1	1	0	1	1	0

Table 4.1: Table with deterministic updating dynamics for rules 182 and 200. The first column gives the rule, while the others give the updating of the central site given its neighbors which are reported in the first row.

As a first remark, we note that this diploid has two absorbing states halting any further configuration development. These are the configurations 0 and 1, as it clearly follows from the fact that both the local rules 200 and 182 associate 1 to the neighbourhood configuration 111 and 0 to the neighborhood configuration 000, see Table 4.1. Moreover, for  $\lambda = 0$ , the diploid reduces to the ECA 200 which is generally considered uninteresting in cellular automata studies because most initial configurations either die out quickly or stabilize into simple, unchanging patterns. As remarked in [16], see also [25, Table 6 on page 540], if the automaton is started with an initial configuration in which zeros and ones are chosen with probability  $1/2$ , then the dynamics reaches a stationary density value equal to  $3/8$ . On the contrary, for  $\lambda = 1$ , the diploid is nothing but ECA 182, which results in a stationary density, independently on the starting configuration, equal to  $3/4$  [25, Figure 12 and page 23] and [26]. We recall that this ECA, although it can produce interesting behaviors, it generally leads to predictable and orderly patterns. Another peculiar feature of the diploid object of our study is observed at  $\lambda = 1/2$ , where the updating dynamics of any site becomes no longer correlated with respect to its neighbors, excepted for the 111 and 000 neighborhood states. Indeed, in all other cases the function  $\phi$  takes values  $1/2$ . In other words, in the absence of long sequences of zeros or ones, sites randomly flip with probability  $1/2$ , so that the stationary density is expected to fluctuate around  $1/2$  [16].

As repeatedly recalled, the diploid 182–200 has been studied in [16], where Mean Field, Monte Carlo simula-

tions, and small block approximations (up to 4) were used to investigate the phase diagram. Here we exploit our algorithmic version of the block approximation to push further the analysis using maximal block size up to 13.

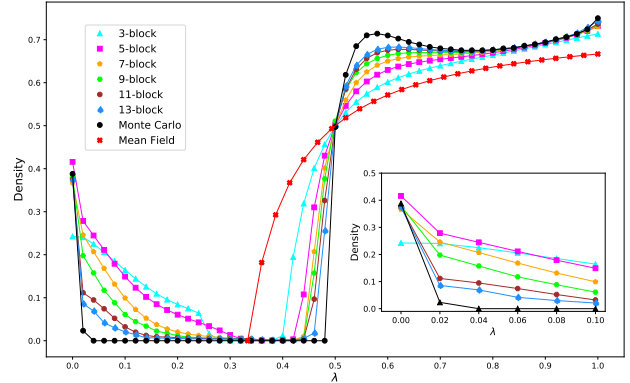


Figure 9: Density profile for the diploid 200-182 as a function of  $\lambda$ . Colour code: Monte Carlo is shown in black, 3-block approximation in cyan, 5-block in magenta, 7-block in orange, 9-block in green, 11-block in brown, and 13-block in blue. For each block approximation, the same randomly initialized density was used; for the Monte Carlo simulations, sites were randomly initialized with density  $1/2$ . The inset is a magnification of the plot within the range  $[0, 0.1]$ .

We summarize briefly the results in [16], Monte Carlo simulations revealed that there is a region in which the stationary state is given by the 0 absorbing state, this happens for  $\lambda$  approximatively in the interval  $(0.03, 0.48)$ . On the other hand, no region in which the 1 absorbing state provides the stationary behaviour is found. For  $\lambda < 0.03$  and  $\lambda > 0.48$  two active regions are detected, meaning that the stationary density is positive. For  $\lambda > 0.48$  the density increases up to the stationary solution  $3/4$  correctly found at  $\lambda = 1$ . The density profile shows a local maximum for  $\lambda$  close to 0.58, an inflection point around 0.62, and a local minimum around 0.75. Mean Field predicts an active state with density  $(3\lambda - 1)/(4\lambda - 1)$  as long as  $\lambda \geq 1/3$ , which means density at  $\lambda = 1$  equal to  $2/3$  (instead of  $3/4$ ), transition point at  $1/3$  (instead of 0.48), and no active state at small values of  $\lambda$ . On the other hand, it correctly predicts the value  $1/2$  for the density at  $\lambda = \frac{1}{2}$ . Finally, it was also remarked that considering block approximation with maximal block size up to 2, 3, 4 provides increasingly better estimates for the critical point and the value of the density at  $\lambda = 1$ .

In this paper, we study the diploid 200-182 using the block approximation with maximal block size up to 13 and in Figure 9 we report, as a function of  $\lambda$ , the density computed within this approximation together with the results of the Monte Carlo simulation. The block approximation recursive equation has been solved iteratively starting from an initial condition in which the maximal block density function was chosen randomly.

To ensure the reproducibility of results, we used the same random initial condition across all simulations. Specifically, the initial block density was generated by drawing uniformly distributed positive values and then normalizing them. We opted for this method to prevent any bias from a specific initial configuration and to simulate a neutral starting point that fairly represents a broad range of possible initial states. In fact, this strategy was chosen to mitigate the risk of the algorithm converging on a distribution with most of its mass on either the zero or the one configuration, which would mirror the absorbing states of 0 and 1 in the diploid. As a result, such an approach allowed us to explore the stationary distribution more effectively.

Overall, higher-order block approximations provide a more accurate description of the Monte Carlo results compared to the low-order. But let us discuss our findings in

detail.

For  $\lambda$  small, unlike Mean Field, the block approximation is able to reproduce the active state found in the Monte Carlo and the steep descent to zero is more and more accurately described when the size of the approximation is increased. We stress that the Mean Field approach was not able to describe the non-trivial behaviour at small values of  $\lambda$ , while the block approximation method proves to be more effective and reliable in the inspection of this domain. We add that the block approximation equations return the solution concentrated on the zero configuration if the solving iterations are initialized with a block matrix close to the Kronecker delta on the zero block configuration. Likewise, starting the iteration with an opposite initialization close to the Kronecker delta on the 1 block configuration, results in a solution concentrated on the 1 block configuration itself.

The existence of the transition at 0.48 is confirmed by the block approximation and the estimate of the transition point is more and more accurate as the order of the approximation is increased. Indeed, for the transition point within the 3-block approximation, we find 0.4, within the 5-block approximation 0.42, within both the 7-block and 9-block approximations 0.44, and within the 11-block and 13-block approximation 0.46.

At the notable point  $\lambda = 1/2$ , as for the Mean Field, all the block approximation-based densities achieve values close to  $1/2$ , confirming the Monte Carlo and the symmetry argument prediction.

The region  $\lambda > 1/2$  is particularly interesting, indeed, the competition between the two local maps defining the diploid produces a not monotonic graph of the stationary density. This behaviour is not at all captured by the Mean Field approximation and is retrieved only by the block approximation with a large maximal block size.

More precisely, all block approximations up to maximal block size 9 show monotonic curves, but a concavity change can be observed at  $\lambda = 0.68$  and  $\lambda = 0.70$  in the 7-block and 9-block cases, respectively. For the 11-block, we observe a local maximum at  $\lambda = 0.62$ , an inflexion point at  $\lambda = 0.67$ , and a local minimum at  $\lambda = 0.74$ .

As said above, all our results have been found solving the iterative equations with precision  $10^{-7}$ . For completeness, we investigate the sensitivity of the block approximation method on the choice of this technical parameter.

Unlike NDECA, where the null rule significantly contrasts with the other rule as  $\lambda$  approaches 0, the diploid 200–182 exhibits, for small  $\lambda$ , an active region. More specifically, ECA 200 is expected to be more prevalent than ECA 182 below the transition value of  $\lambda$ . Consequently, the dynamics approaches some stationary state made of bulks of ones and zeros. In such a scenario, the presence of ECA 182 allows for the flipping of a single site within one bulk, causing the collapse of that block to zero when ECA 200 is applied subsequently. As a result, the dynamics fall into the null absorbing state as the contrast between the two rules is mild (say,  $\lambda$  around 0.3), while non-null stationary measures become more prevalent as the contrast becomes weaker (say,  $\lambda$  close to zero). Heuristically, we can say that this contrast may prematurely halt the iterative search of block approximation algorithms. This occurs because ECA 182 may not be selected frequently enough to guide the search towards the Monte Carlo solution.

In figure 10 the 3-block approximations are shown at various levels of precisions. Specifically, we explored the level of precisions from a maximum of  $10^{-3}$  up to a minimum of  $10^{-20}$ . As for the analysis of Figure 9, we used the same initial conditions for each run to give this analysis more reproducibility. As expected, the accuracy of the block approximation improves as the algorithm's precision decreases. Such an improvement is particularly noticeable away from  $\lambda = 0$ , where the transition from the equilibrium state of ECA 200 to the null absorbing state is better captured when higher precision levels are selected for the block approximation. In the region  $\lambda > 1/2$  the precision  $10^{-4}$  is already sufficient to get very precise solutions of the iterative equations, on the other hand in the region close to 0 the precision should be pushed to  $10^{-15}$ . Thus, we have to conclude that in this region the curves discussed in Figure 9 are only qualitatively reliable.

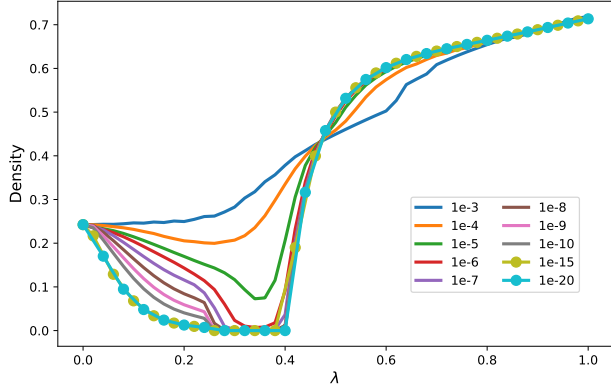


Figure 10: Sensitivity analysis of the 3-block approximation with respect to the precision of the algorithm. Colored lines show approximations at different values of of precision

## 5. An example of one-dimensional totalistic PCA

In this section, we consider the model which is the main object of study in [22]. It is an example of totalistic PCA, namely, a PCA in which the one-site updating probability  $p_i(\cdot|x)$  depends only on the total of the values of the cells in the neighborhood  $I_i$ , namely, on  $\sigma_i(x) = x_{i-1} + x_i + x_{i+1}$ . From our point of view, the interest of the model is twofold: i) it shares with the diploid studied in Section 4 the property that it admits two absorbing states, i.e., 0 and 1; ii) it is an example of probabilistic mixtures of four ECA. In this complicated setup we show the ability of the block approximation to provide a very precise description of a highly non-trivial phase diagram.

Following [22] and recalling the notation introduced in Section 2.1 the totalistic PCA is defined by saying that the cell variable at time  $t$  is set to 0 if  $\sigma_i(\zeta^{t-1}) = 0$ , to 1 if  $\sigma_i(\zeta^{t-1}) = 3$ , and it is chosen by performing a Bernoulli trial with parameter  $q_s$  if  $\sigma_i(\zeta^{t-1}) = s$ , with  $s = 1, 2$ , and  $q_1, q_2 \in [0, 1]$ . This is equivalent to say that the one-site updating probability are the following

$$\begin{aligned}
 p_i(1|000) &= 0, \\
 p_i(1|001) &= p_i(1|010) = p_i(1|100) = q_1, \\
 p_i(1|011) &= p_i(1|101) = p_i(1|110) = q_2, \\
 p_i(1|111) &= 1,
 \end{aligned} \tag{5.17}$$

for any  $i \in \Lambda_n$ , where we misused the notation introduced in (2.3) by reporting on the right of the bar only the neighborhood configuration.

	111	110	101	100	011	010	001	000
<b>254</b>	1	1	1	1	1	1	1	0
<b>232</b>	1	1	1	0	1	0	0	0
<b>150</b>	1	0	0	1	0	1	1	0
<b>128</b>	1	0	0	0	0	0	0	0

Table 5.2: Local rules used in the definition of the model in Section 5. The first column reports the local rule decimal code, while the others report the updating of the central site given its neighbors which are listed in the first row.

It is very interesting to remark that this model can be rewritten as the probabilistic mixture of ECA (2.3)–(2.4) of the four local rules 254, 232, 150, 128, respectively, as the maps  $f_1, f_2, f_3, f_4$  in (2.4) with the four reals  $\xi_1, \dots, \xi_4 \in [0, 1]$  satisfying the equations

$$\xi_1 + \xi_2 = q_2, \quad \xi_1 + \xi_3 = q_1, \quad \xi_1 + \xi_2 + \xi_3 + \xi_4 = 1, \tag{5.18}$$

and the four local rules considered above detailed in Table 4.1. Indeed, (5.17) are recovered noting that from (2.3) and (2.4) one has  $p_i(1|x) = \phi(x) = \sum_{r=1}^4 \xi_r f_r$ , and thus

$$\begin{aligned}
 p_i(1|000) &= 0, \\
 p_i(1|001) &= p_i(1|010) = p_i(1|100) = \xi_1 + \xi_3, \\
 p_i(1|011) &= p_i(1|101) = p_i(1|110) = \xi_1 + \xi_2, \\
 p_i(1|111) &= \xi_1 + \xi_2 + \xi_3 + \xi_4.
 \end{aligned}$$

Finally, we remark that the system of equations (5.18) is compatible in  $[0, 1]$  and a solution can be written as follows:

$$\begin{aligned}
 \xi_1 &= q_1, \xi_2 = q_2 - q_1, \xi_3 = 0, \xi_4 = 1 - q_2 & \text{if } q_1 < q_2, \\
 \xi_1 &= q_1, \xi_2 = \xi_3 = 0, \xi_4 = 1 - q_1 & \text{if } q_1 = q_2, \\
 \xi_1 &= q_2, \xi_2 = 0, \xi_3 = q_1 - q_2, \xi_4 = 1 - q_1 & \text{if } q_1 > q_2.
 \end{aligned}$$

The Mean Field computation in [22] provides for the stationary density the solutions 0, 1, and  $\delta(q_1, q_2) = (3q_1 - 1)/(1 + 3q_1 - 3q_2)$ . The last one is meaningful, namely, it takes values in  $[0, 1]$ , only for  $q_1 \geq 1/3$  and  $q_2 \leq 2/3$ . Since  $\delta(1/3, q_2) = 0$  and  $\delta(q_1, 2/3) = 1$ , we can say that the Mean Field approximation predicts the following phase diagram in the square  $[0, 1] \times [0, 1]$ : the absorbing states 0 and 1 are

respectively the stationary states in the region  $q_1 < 1/3$  and  $q_2 < 2/3$  and in the region  $q_1 > 1/3$  and  $q_2 > 2/3$ . On the other hand, in the domain  $1/3 \leq q_1$  and  $2/3 \geq q_2$  the stationary density is provided by the continuous function  $\delta(q_1, q_2)$ . Nothing can be said in the squared region  $q_1 < 1/3$  and  $q_2 > 2/3$ .

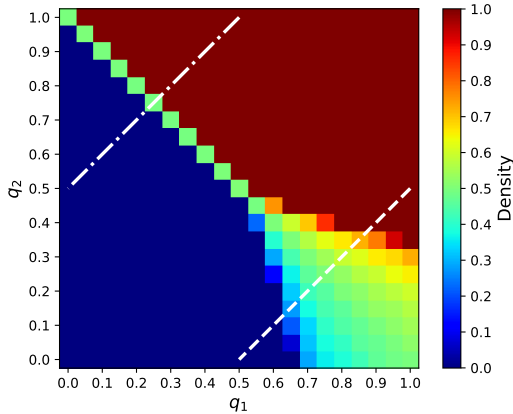


Figure 11: Monte Carlo simulation of the one-dimensional totalistic PCA. Parameters  $q_1$  and  $q_2$  are shown along the horizontal and vertical axes, respectively. The heatmap shows the density for a given couple of parameters  $(q_1, q_2)$  on a grid of  $21 \times 21$  points in  $[0, 1] \times [0, 1]$  with spacing 0.05. The dashed-dotted and the dashed lines represent respectively the line of equations  $q_2 = q_1 + 1/2$  and  $q_2 = q_1 - 1/2$ .

The Monte Carlo density prediction, which is in perfect agreement with that reported in [22, Figure 3], is shown in Figure 11. Simulations were accomplished on a 10000-length array throughout 10000 iterations. Monte Carlo simulations reveal a scenario that confirms only partially the Mean Field predictions. In particular, close to the point  $q_1 = 0$  and  $q_2 = 1$ , we observe a discontinuous transition between the 0 and 1 states, indeed the density has an abrupt jump from 0 to 1. More precisely, this discontinuous transition is observed through the line  $q_1 + q_2 = 1$  for  $q_1 \in (0, 1/2)$ .

It is interesting to remark that, exactly on the line  $q_1 + q_2 = 1$  with  $q_1 \in (0, 1)$ , the observed value for the stationary density is  $1/2$ . This fact is not surprising since for this choice of the parameters the totalistic model reduces to the diploid studied in Section 4 at  $\lambda = 1/2$ .

The discontinuous transition dies out at  $q_1 = 1/2$  where the discontinuous transition line bifurcates and gives rise to two curves, symmetric with respect to the line  $q_1 + q_2 = 1$ , where a continuous transition between, respectively, the 0 and 1 absorbing states and a continuous phase with positive density are observed.

In order to study this interesting phase diagram with the block approximation to confirm the Monte Carlo results both in the discontinuous and continuous transition regions, we have explored the model along the lines  $q_2 - q_1 = 1/2$  and  $q_2 - q_1 = -1/2$  (see the dotted dashed and dotted lines in Figure 11).

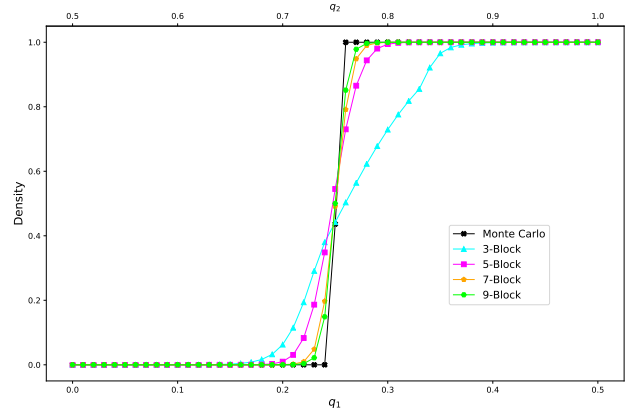


Figure 12: Stationary density along the line  $q_2 - q_1 = 1/2$ . In cyan the 3-block, in magenta the 5-block, in orange the 7-block, and in green the 9-block approximation. In black the Monte Carlo simulation. On top and on the bottom axes, the values of  $q_2$  and  $q_1$  are respectively reported.

In Figure 12, Monte Carlo and block approximation estimates for the stationary density along the line  $q_2 - q_1 = 1/2$  are shown. The model exhibits a discontinuous transition, from the quiescent zero density state to the active density one state at  $q_1 = 1/4$ , or equivalently,  $q_2 = 3/4$ . This behaviour is clearly captured by the Monte Carlo simulations and it is clearly confirmed by a careful analysis of the block approximation results. The 3-block approximation predicts a very smooth change from the quiescent to the active state and the transition point can be estimated at  $q_1 = 0.18$  (or  $q_2 = 0.68$ ). A more sudden change is observed with the 5-block approximation and the transition point estimate becomes  $q_1 = 0.2$  (or  $q_2 = 0.7$ ). The density

curves computed with the 7-block and 9-block are almost perfectly overlapped: the description of the sharp transition is more accurate and the transition point is estimated at  $q_1 = 0.22$  (or  $q_2 = 0.72$ ).

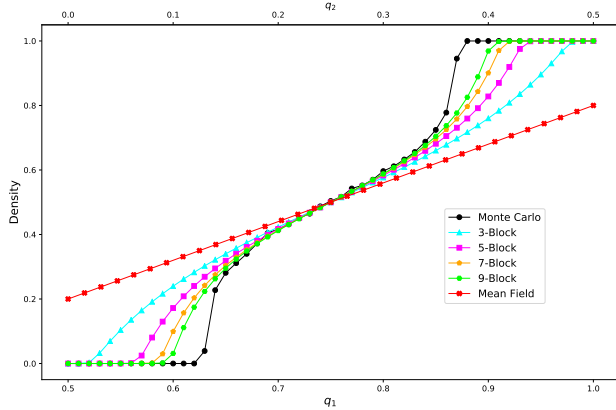


Figure 13: Stationary density along the line  $q_2 - q_1 = -1/2$ . In red the Mean Field computation. In cyan the 3-block, in magenta the 5-block, in orange the 7-block, and in green the 9-block approximation. In black the Monte Carlo simulation. On top and on the bottom axes, the values of  $q_2$  and  $q_1$  are, respectively, reported.

In Figure 13, Mean Field, Monte Carlo, and block approximation estimates for the stationary density along the line  $q_2 - q_1 = -1/2$  are reported. The Monte Carlo estimate of the stationary density reveals the presence of two continuous transitions between the two absorbing states, namely, 0 and 1, and a continuous phase with positive density. The two transition points are close to  $q_1 = 0.63$  (or  $q_2 = 0.13$ ) and  $q_1 = 0.87$  (or  $q_2 = 0.37$ ). In between, the stationary density varies smoothly. The Mean Field approximation is not able to capture the two continuous transitions, although the agreement with the Monte Carlo results is good close to  $q_2 = 3/4$  where the line  $q_2 - q_1 = -1/2$  intersect the  $1/2$  density line  $q_1 + q_2 = 1$ .

On the other hand, block approximations provide a precise description of the two continuous transitions. Indeed, the agreement between Monte Carlo and block approximation prediction is perfect in the centre part of the graph, namely, around  $q_1 = 0.75$  (or  $q_2 = 0.25$ ). On the other hand, when the transition point is approached, the block approximation curves depart from the Monte Carlo den-

sity prediction, but the estimate of the transition points get better and better when the size of the maximal block is increased. More precisely, for what concerns the transition point involving the quiescent 0 state, the 3-block, 5-block, 7-block, 9-block, respectively, predicts  $q_1 = 0.52$ ,  $q_1 = 0.56$ ,  $q_1 = 0.58$ , and  $q_1 = 0.59$ . On the other hand, for the transition point involving the active 1 state, the analogous sequence is  $q_1 = 0.97$ ,  $q_1 = 0.94$ ,  $q_1 = 0.92$ , and  $q_1 = 0.91$ .

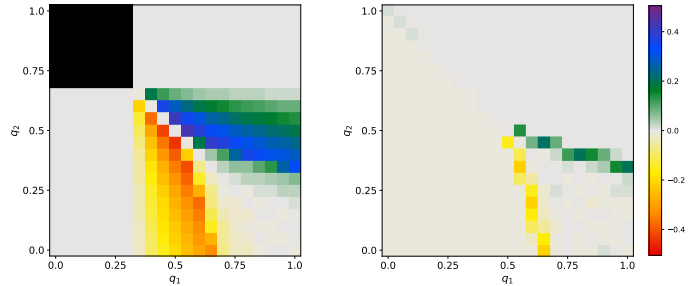


Figure 14: Difference between the stationary density measured with the Monte Carlo simulation and the Mean Field approximation on the left and between the Monte Carlo simulation and 7-block approximation on the right. As in Figure 11 the heatmap shows the measured quality for a given couple of parameters  $(q_1, q_2)$  on a grid of  $21 \times 21$  points in  $[0, 1] \times [0, 1]$  with spacing 0.05. In the black region on the left, the Mean Field solution is not acceptable.

In Figures 12 and 13, we have evaluated the effectiveness of the block approximation in describing the transitions observed via Monte Carlo simulations. Our findings confirm that the phase diagram of the model is highly non-trivial, exhibiting both continuous and discontinuous transition lines that converge at the point  $(1/2, 1/2)$ . As a final remark, we demonstrate that the block approximation can predict the stationary value of the density with acceptable precision across the entire parameter space  $[0, 1] \times [0, 1]$ . Additionally, we emphasize that it improves upon Mean Field results even when not excessively large maximal blocks are used. Indeed, in Figure 14 we plot the difference between the stationary density measured with the Monte Carlo simulation and the Mean Field approximation on the left, and between the Monte Carlo simulation and the 7-block approximation on the right. As usual, the iterative equations are solved with a precision of  $10^{-7}$ . The

figure clearly shows that the block approximation is much more reliable than the Mean Field computation. Moreover, errors (which can be reduced by increasing the size of the maximal block) in estimating the stationary density are detectable only very close to the continuous transition lines.

## 6. Conclusions

This work aimed to compare the effectiveness of a crude implementation of block approximation with respect to other approaches, such as Monte Carlo and Mean Field, in describing the phase diagram of a PCA. We studied several cases with increasingly complex dynamics, including the NDECA, the diploid with local rules 200-182, and an example of totalistic probabilistic PCA.

Overall, the Mean Field approach, while computationally efficient and straightforward, often fails to capture the dynamical features and the transitions between different stationary states. In contrast, the block approximation, although more computationally intensive, always provides a more accurate and detailed representation for all PCAs considered. In some cases, successfully identifying transitions was possible even with a low-order block approximation.

Regarding NDECAs, all results supported the ability of block approximation to accurately reproduce their dynamics compared to the Mean Field approach. For instance, in the case of NDECA 202, the block approximation successfully reproduced the transition, a feature not captured by the Mean Field approach. Similarly, for NDECA 234, the Mean Field approach predicted a phase transition not observed in Monte Carlo simulations. The block approximation, however, showed no phase transition and aligned well with Monte Carlo behaviour as larger blocks were included in the analysis. The case of NDECA 120 exemplified a scenario where the Mean Field predicted a phase transition that did not actually occur. Here, the block approximation revealed an apparent phase transition. However, upon inspecting the block probabilities, it became evident that this apparent transition was likely the result of artefacts induced by the approximation method. In the case of NDECA 222, the block approximation closely approximated the transition point, matching the Monte Carlo results where the Mean Field approach diverged significantly.

Exploring the dynamics of the diploid 200-182 enabled

us to examine the performance of the block approximation method, still in our raw version, in the context of a more intricate diploid, which does not include the null rule and in the presence of two absorbing states. Initially, we noted that the block approximation accurately replicated the behaviour of the active region near  $\lambda = 0$ , a result unexpected by the Mean Field approach. Additionally, the block approximation provided interesting results in the region above the transition point, when the predictable structures of the local 182 become slightly more relevant than those of the local rule 200. We also observed that, increasing the order of the approximation, a better estimate of the transition point and a better match with the Monte Carlo density profile was found. Applying the block approximation to the totalistic probabilistic PCA revealed that it can lead to very accurate descriptions. Unlike the Mean Field approach, which did not identify any transition along the line  $q_2 - q_1 = -1/2$ , the block approximation revealed the presence of a discontinuous transition. Specifically, the block approximation revealed to be able to capture the complicated structure of the phase diagram in which two continuous transitions are present. Overall, the analysis of the Mean Field and block approximation methods highlight the trade-off between computational feasibility and accuracy. The Mean Field approach, intended as a useful initial analysis tool can quickly provide insights into the general behavior of PCAs within a theoretical framework. However, our analysis emphasizes that this approach might lead to erroneous predictions, either missing transitions where they exist or predicting them where they do not. A simple crude implementation of the 3-block approximation offers a practical solution to outline the system phase diagram without involving complex and time-consuming computations. For a more precise and comprehensive understanding, particularly in systems exhibiting complex phase transitions, the block approximation proves to be a valuable tool. Combining both approaches allows for a balance of efficiency and accuracy, employing the Mean Field approach for broad theoretical overviews and the block approximation for detailed investigations.

## Acknowledgements

ENMC and GL thank the PRIN 2022 project “Mathematical Modelling of Heterogeneous Systems (MMHS)”, financed by the European Union - Next Generation EU, CUP B53D23009360006, Project Code 2022MKB7MM, PNRR M4.C2.1.1.

The authors have nothing to declare

## Declaration of interests

## Declaration of generative AI in scientific writing

The authors declare that no generative AI and AI-assisted technologies have been utilized during the writing process of this manuscript.

## References

- [1] R. Fernandez, P.-Y. Louis, and F.R. Nardi. Overview: Pca models and issues. In P.-Y Louis and F. R. Nardi, editors, *Probabilistic Cellular Automata: theory, applications and future perspectives*, pages 1–30. Springer International Publishing, 2018.
- [2] C.A. Valentim, J.A. Rabi, and S.A. David. Cellular-automato model for tumor growth dynamics: virtualization of different scenarios. *Computers in Biology and Medicine*, 153:106481, 2023.
- [3] P. Davis. Does new physics lurk inside living matter? *Physics Today*, 73(8):34, 2020.
- [4] S. Wolfram. Statistical mechanics of cellular automata. *Rev. Mod. Phys.*, 35:601–644, 1983.
- [5] S. Wolfram. Computation theory of cellular automata. *Comm. Math. Phys.*, 96:15–57, 1984.
- [6] N. Fatès. Diploid cellular automata: First experiments on the random mixtures of two elementary rules. *Lectures Notes in Computer Science*, 10248:97–108, 2017.
- [7] A. Busic, J. Mairesse, and I. Marcovici. Probabilistic cellular automata, invariant measures, and perfect sampling. *Adv. in Appl. Probab.*, 45:960–1980, 2013.
- [8] A. Toom. *Contours, convex sets and cellular automata*. IMPA mathematical publications, 2004.
- [9] J. Mairesse and I. Marcovici. Around probabilistic cellular automata. *Theoretical Computer Science*, 559:42–72, 2014.
- [10] J.R.G. Mendonça. Monte carlo investigation of the critical behavior of stavskaya’s probabilistic cellular automaton. *Phys. Rev. E*, 83:42–72, 2011.
- [11] D. Dhar. Exact solution of a directed-site animals-enumeration problem in three dimensions. *Phys. Rev. Lett.*, 51:853–856, 1983.
- [12] H.A. Gutowitz, J.D. Victor, and B.W. Knight. Local structure theory for cellular automata. *Physica D*, 28:18–48, 1987.
- [13] H.A. Gutowitz and J.D. Victor. Local structure theory in more than one dimension. *Complex Systems*, 1:57–68, 1987.
- [14] H. Fukś and N. Fatès. Local structure approximation as a predictor of second order phase transitions in asynchronous cellular automata. *Natural computing*, 14:507–522, 2015.

- [15] H. Fukś. Construction of local structure maps for cellular automata. *J. Cell. Automata*, 7:455–488, 2012.
- [16] J.R.G. Mendonça and M.J. de Oliveira. An extinction-survival-type phase transition in the probabilistic cellular automaton p182–q200. *Journal of Physics A: Mathematical and Theoretical*, 44:155001, 2011.
- [17] A. Pelizzola. Cluster variation method in statistical physics and probabilistic graphical models. *J. Phys. A: Math. Gen.*, 38:R309, 2005.
- [18] E.N.M. Cirillo, G. Gonnella, and A. Pelizzola. Folding transition of the triangular lattice in a discrete three-dimensional space. *Physical Review E*, 53:3253, 1996.
- [19] E.N.M. Cirillo, F.R. Nardi, and C. Spitoni. Phase transitions in random mixtures of elementary cellular automata. *Physica A*, 573:125942, 2021.
- [20] C. Maes and S. Shlosman. Ergodicity of probabilistic cellular automata: A constructive criterion. *Communication in Mathematical Physics*, 135:233–251, 1991.
- [21] C. Maes and S. Shlosman. When is an interacting particle system ergodic? *Communication in Mathematical Physics*, 151:447–466, 1993.
- [22] F. Bagnoli, N. Boccara, and R. Rechtman. Nature of phase transitions in a probabilistic cellular automaton with two absorbing states. *Physical Review E*, 63:046116, 2001.
- [23] R. Kikuchi. Superposition approximation and natural iteration calculation in cluster-variation method. *J. Chem. Phys.*, 60:1071–1080, 1974.
- [24] L. Taggi. Critical probabilities and convergence time of percolation probabilistic cellular automata. *Journal of Statistical Physics*, 159:853–892, 2015.
- [25] S. Wolfram. *Cellular automata and complexity: collected papers*. crc Press, 2018.
- [26] P. Grassberger. New mechanism for deterministic diffusion. *Physical Review A*, 28:3666, 1983.